BJRS

BRAZILIAN JOURNAL
OF
RADIATION SCIENCES
09-01A (2021) 01-16

Characterization of bi-layers formed over maraging steel 300 during aging process with steam atmosphere by GIXRD and SEM

Silva[a] V.S.P., Neto[a] J.R.F., Oliveira[a] D.C., Silva[a] S.L.F., Camargo[a] F.

[a] *AMAZUL – Amazônia Azul Tecnologias de Defesa S.A., 05.581-001, São Paulo-SP, Brazil*

vanessa.sanches@marinha.mil.br

ABSTRACT

Maraging steels are martensitic steels hardened by precipitation during thermal aging, with good machining properties and high strength and corrosion resistance. It is well suited for applications which require high strength-to-weight material, being used in aerospace, aeronautics, and nuclear industries. A protective and corrosion resistant oxide layer can be formed during age hardening if treated in steam atmosphere. This work aims to use grazing incidence X-ray diffraction (GIXRD) to evaluate qualitatively the thickness of the layers formed during this process. GIXRD and scanning electron microscopy (SEM) were employed to identify and order the layered structure formed on four specimens of maraging steel grade 300 with different surface finishes that were previously solution annealed twice at (950 ± 5) °C for 1 h, air-cooled, and submitted to oxidation process under positive pressure around 1.5 kPa of steam at (480 ± 5) °C for 6 h followed by forced air cooling. The diffraction patterns were measured employing CuK$_\alpha$ radiation and parallel beam, in step scan mode, using incident angles varying from 0.2º to 4.0º and 20º < 2θ < 85º. The results revealed the formation of two layers, the innermost was formed by γ-iron (austenite – fcc) phase followed by a mixture of oxides (hematite and magnetite) on the top, regardless of surface finish, which was confirmed by the SEM analysis that also allowed the measurement of the average layer's thickness of oxides (1.130 ± 0.094) µm and austenite (0.507 ± 0.090) µm phases, and corroborated the qualitative thicknesses analysis made from GIXRD results.

Keywords: **Maraging Steel, Grazing Incidence X-ray Diffraction, Scanning Electron Microscopy.**

ISSN: 2319-0612
Accepted: 2020-12-30

1. INTRODUCTION

Maraging steels are low-carbon martensitic steels which employ substitutional alloying elements to achieve precipitation strengthening (age-hardening). The rare combination of good machining properties and high strength, high fracture toughness and high corrosion resistance found in maraging steels make them well suited for applications which require high strength-to-weight material, such as aircraft parts and rocket motor case, tooling applications and nuclear plants [1-4]. If the thermal age-hardening process is done in steam atmosphere, a protective and corrosion resistant oxide layer will be formed over the bulk, which is an advantage of cost and efficiency comparing with other types of coating protection layers [4].

The knowledge about the structure of the layer formed on the bulk, and its thickness are the first step to analyze the corrosion protection and better understand the mechanisms of steam oxidation of maraging steel 300 (MA300). Although some previous studies already showed indicatives of layered structure [4-7], and evaluate the thickness using X-ray diffraction wasn't a simple task [8], this work aims to use grazing incidence X-ray diffraction (GIXRD) as a non-destructive method to evaluate qualitatively the average layer thickness, and identify and order the phases formed over the bulk during the oxidation process.

Generally, analysis of thicknesses and multilayer systems by GIXRD study in details differences of penetration depth and the average information depth considering not only the geometry and the incidence angle, but also the attenuation of X-ray beam along the sample, and its dependence on phase distribution throughout the X-ray beam path [9-12]. However, this work proposes a simplified analysis that involves just geometrical considerations to achieve comparative and qualitative information among the layers.

In GIXRD the diffraction pattern is collected keeping the X-ray tube fixed while the detector's goniometer scans. The smaller the incidence angle (θ_{inc} – angle between the incident X-ray beam and the specimen surface), the shallower penetration depth of X-rays, which means that as θ_{inc} increases, the observed data come from deeper specimen's layers [9, 13].

Simplifying this effect, Figure 1 compares two parallel beams with the same width radiating samples in different incident angles, $\theta_{inc} < \theta'_{inc}$. Considering no significant change in absorption

factor among the phases, the same penetration length (d) clearly implicates in different observation depths.

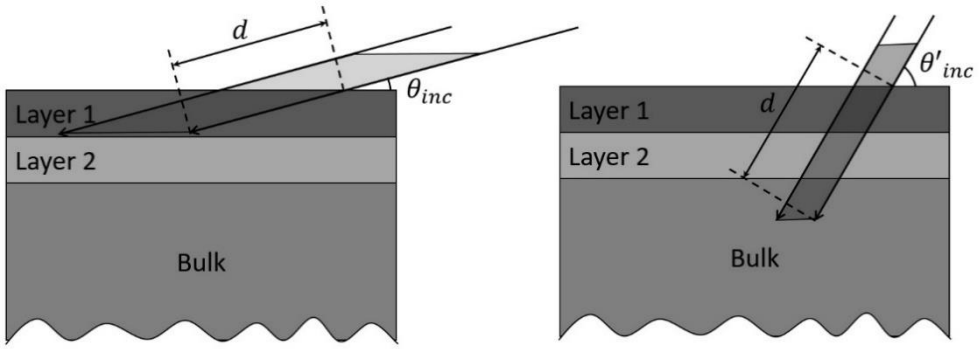

Figure 1: *Schematic differences between the average depth where the signal collected comes from in GIXRD using parallel beam, between* $\theta_{inc} < \theta'_{inc}$.

This geometric fact aforementioned associated to the observation that a change in the incidence angle for lower angles results in a higher variation to the depth analyzed ($\Delta \boldsymbol{h}$) when comparing to the same change for higher angles, as can be seen in Figure 2, will be used to qualitatively and comparatively assess the thickness of the layers formed during the oxidation process of the MA300.

In addition, the specimen's cross-section will be observed by scanning electron microscope (SEM) to measure the thickness of each layer and to compare with the conclusions extracted from GIRXD technique, clarifying its limitations and scope for this case under study.

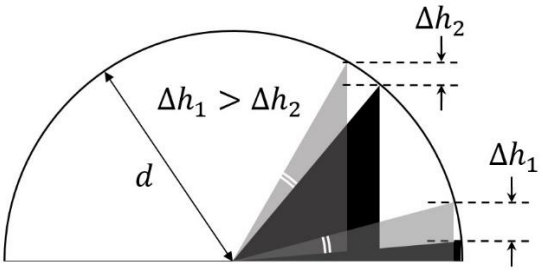

Figure 2: *Diagram showing that for same angular variation, represented by double line white arc, the depth variation is bigger for lower incidence angles* (Δh_1) *than for higher ones* (Δh_2).

2. MATERIALS AND METHODS

2.1. Specimens preparation

In this work, four samples of maraging steel grade 300 were cut to dimensions of approximately 40 × 20 × 5 mm, defined so that the incidence angle could reach only the specimen even in a minimum value of 0.2°, during the GIXRD measurements. Then, by employing a muffle furnace they were solution annealed twice at (950 ± 5) °C for 1 h [2, 14] and air cooled, in order to homogenize the alloy matrix.

Before thermal aging, the specimens received different surface finishes: two of them were mechanically sanded to 1200 grit, and the others were polished with diamond paste down to 1 μm to have a mirrored surface (no scratches). The specimens were then submitted to oxidation process under positive pressure around 1.5 kPa of steam at (480 ± 5) °C for 6 h [2, 14] followed by air cooling to room temperature using a Lindberg/MPH Steam Homo® Pit furnace model 12-HC-1416-HST-12. One pair of sanded and polish specimens were treated on furnace top basket and received the names of **T**op **S**anded (TS) and **T**op **P**olish (TP) specimens, and the others were treated on furnace bottom basket, and will be called **B**ottom **S**anded (BS) and **B**ottom **P**olish (BS) specimens.

2.2. GIXRD analysis

Diffraction patterns were measured employing CuK_α ($\lambda = 1.5406$ Å) radiation in a Bruker diffractometer model D8-Advance, equipped with a XYZ motorized holder that allowed precise alignment of the sample and a Göbel mirror for parallel beam optics. The incidence angles varied from 0.2º to 1.0º in steps of 0.2º and from 1.0º to 4.0º in steps of 0.5º. The data were collected in step scan mode, ranging $20º < 2\theta < 85º$.

Before each test an alignment procedure was executed, first correcting the high (z-value) of the specimen, by positioning the X-ray source in front of the detector ($\theta_{X-ray} = \theta_{detector} = 0°$), so parallel beam focuses directly onto the detector, that was protected by a copper filter, and performing a z-scan. While the sample is increasing its position along the z-axes, the intensity of the detected X-ray varies from a maximum value, corresponding to the entire beam incident to the detector, to a

minimum value when the sample totally blocks the beam. The position related to the average intensity measured was then set to zero-position.

Then, the inclination of the sample was verified by performing a rocking scan. During this scan, X-ray tube and detector stay one in front of each other ($\theta_{X-ray} = -\theta_{detector}$) and vary around 0º (for example, $-2.0° < \theta_{X-ray} < 2.0°$). When the surface of the sample is in the same direction as the beam, the intensity counted is a maximum, so the angle θ related to the maximum intensity measured was set to zero degree.

The two steps described above need to be performed at least twice to guarantee the accuracy of the measurements, especially those related to incidence angle values, because it was necessary to increase the signal-to-noise ratio affected by the presence of iron and its consequent fluorescence due to copper radiation and by the very low incident angles. But, in practice, these procedures were repeated until it was possible to confirm that the z-position related to the average beam still at the same value, and the maximum signal measured during rock scan matches to zero degree, i.e., the alignment was completed and checked.

2.3. SEM analysis

The specimens were cut and mounted with bakelite and edge retention resin in a way that normal section of the oxide surface could be observed, besides avoiding bulging at the edges of the samples. Then they were ground and polished down to 1 μm of diamond solution and chemically etched by immersion in a solution of 10 g of potassium metabisulfite, 15 g sodium bisulfite and 50 ml of water.

After etching, by employing a model Axio Imager M2m Carl Zeiss microscope, optical observation was made to verify the homogeneity of the layers, since the signal of XRD analysis is an average of the whole surface measured, and the thickness measurements from the SEM would be made in a small portion of the sample. Although the optical images showed some defects and a bit undulate surface, it was in average very consistent, and because of that only two magnifications (10,000 and 15,000) for each specimen were used to evaluate the thickness by SEM.

SEM analysis were performed through Carl Zeiss scanning electron microscope, model EVO® MA15. The specimens were examined using secondary electrons (SE) and backscattering electrons (BSE) detectors, but only the micrographs obtained by means of the latter were used to measure the

average thickness of the layers observed, due to the better contrast obtained between the oxide and the metal phases (Z-contrast). So, the mean was taken from the measurement of 12 equally spaced positions of the two micrographs taken by BSE detector.

3. RESULTS AND DISCUSSION

3.1. GIXRD results

In this section we will present the main GIXRD patterns that were used to support the conclusions described here. In all specimens investigated the same number of phases and sequence of layers were identified, starting with an outermost oxide layer (Figure 3).

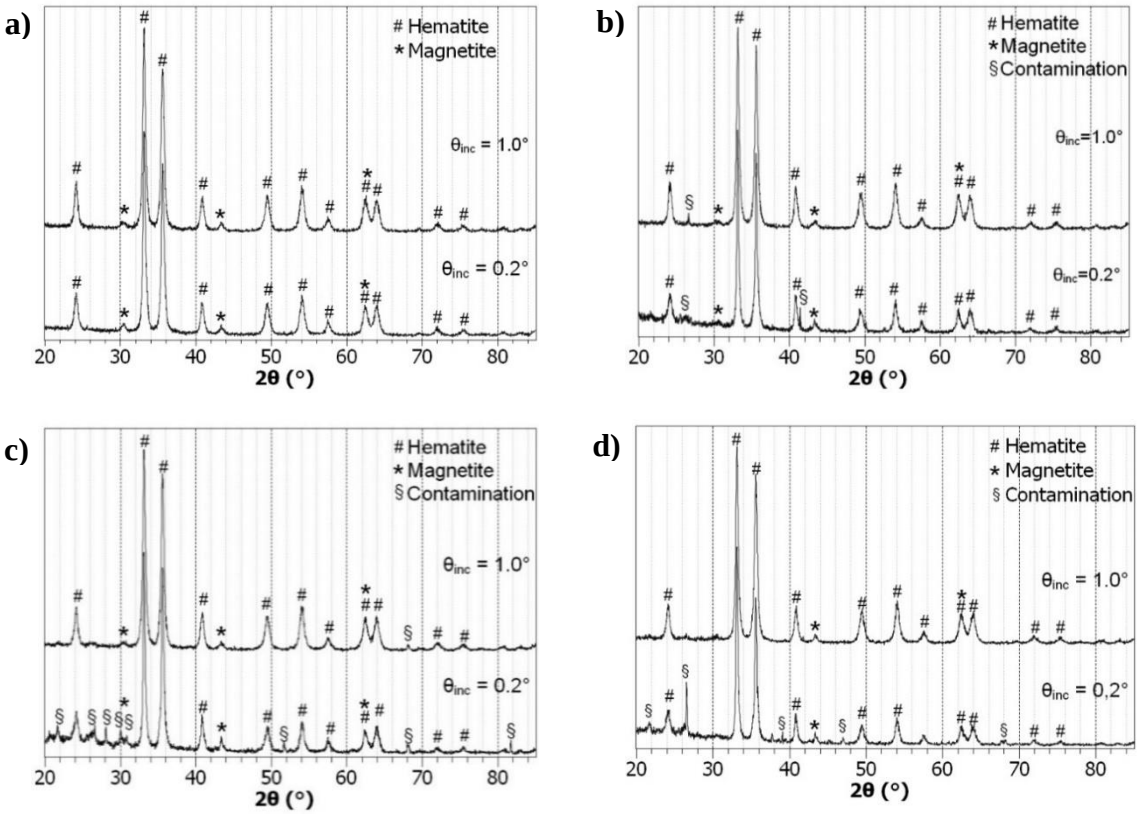

Figure 3: *GIXRD patterns of a) TP, b) TS, c) BP and d) BS specimens for angles of incidence 0.2° and 1.0°.*

Therefore, and since as bigger the incidence angle goes as deeper the signal comes from, it was possible to identify a first top layer composed by a mixture of Hematite and Magnetite (Figure 3), in which last phase increased with the depth of the layer. Then an austenite phase (Figure 4) was identified by an iron face centered cubic (fcc) cell, followed by a deeper martensite phase (Figure 5), that was characterized as an iron body centered cubic (bcc) cell and related to the bulk.

Figure 3 shows the results of 0.2° and 1.0° of incidence angle to the four specimens. The patterns of incidence angles of 0.4°, 0.6° and 0.8° were omitted because they show only the evolution from the patterns of 0.2° to 1.0° with no extra information, which means that no extra peaks appeared in the omitted patterns. Observing Figure 3, it is possible to realize that the patterns didn't differ too much, and the 0.2° results are comparable with the 1.0° patterns for all specimens analyzed here.

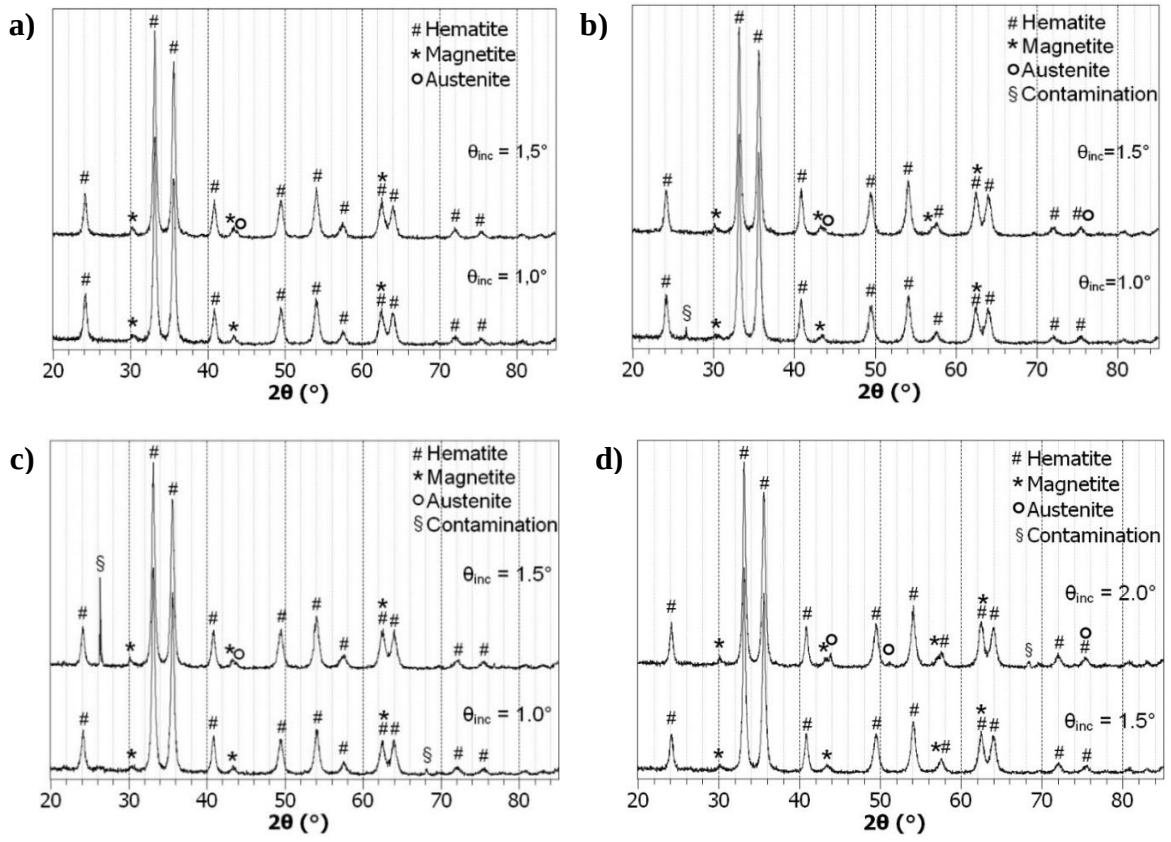

Figure 4: *GIXRD patterns of a) TP, b) TS, c) BP and d) BS specimens showing the first signal of the main reflection (1 1 1) of austenite phase.*

A slightly increase of magnetite signal was noticed as the incidence angle rises, while the hematite signal remains the same (compare Figures 4 and 5 for example). Maybe this fact reveals that the magnetite was formed before the hematite in the oxide layer, because although it was not possible to separate the hematite from the magnetite phases into two staked layers, the oxide mixture appears to have different composition depending on the depth, being the magnetite mostly present in deeper layers, i.e., bigger incidence angles, which could be confirmed by further studies.

The samples BS and BP present more contamination signal, especially for the lowest angles of incident (superficially). This contamination probably comes from the powder ceramic insulation of the furnace, and are composed of silicates and alumina, as proved by XRD pattern measured of a sample of powder collected inside the oven but not showed here, since this analysis was made only to understand why some phases, not theoretically predicted, had appeared in some measurements with shallower angles.

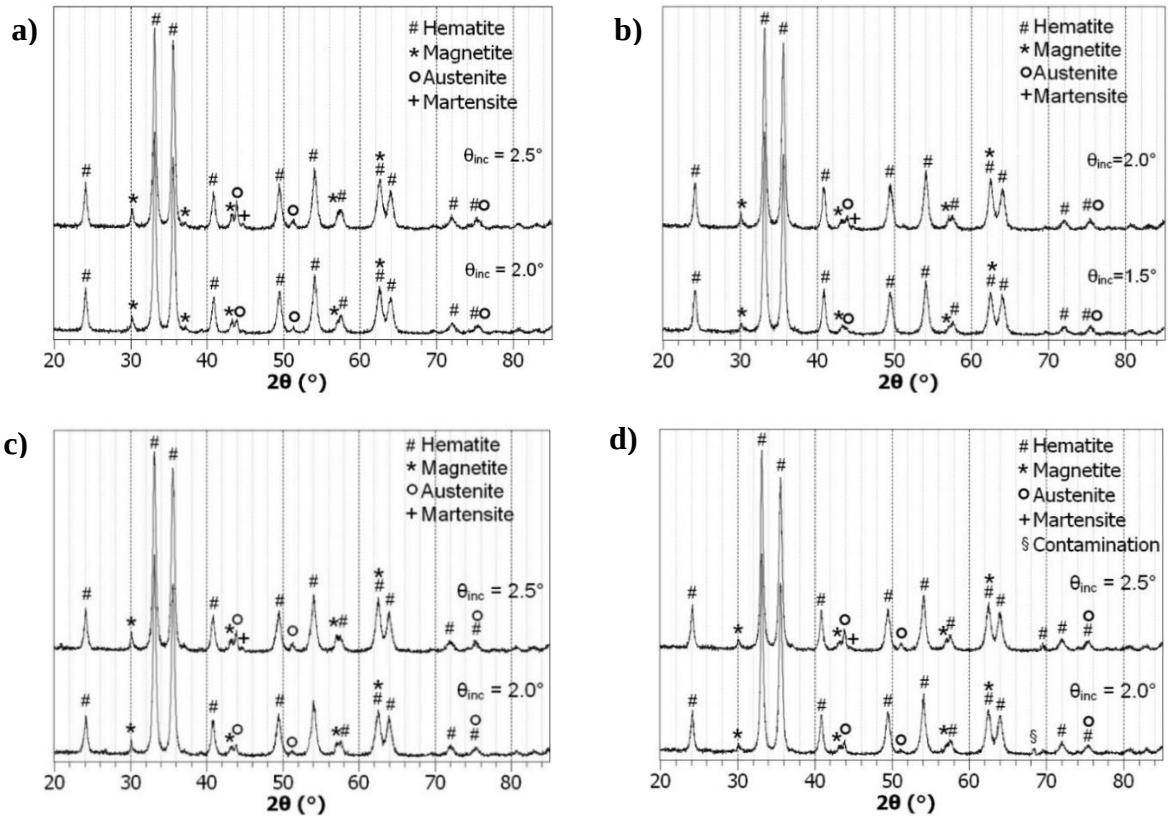

Figure 5: *GIXRD patterns of a) TP, b) TS, c) BP and d) BS specimens showing the first signal of the main reflection (1 1 0) of martensite phase.*

Figures 4 and 5 show the first appearance of austenite and martensite phases in GIRXD patterns, respectively. Because of the low signal-to-noise ratio of the measurements, produced by the combination of X-ray fluorescence of iron, geometry used and quite irregular surface finish of the samples after the aging treatment, the threshold used to decide in which angle the phases were first identified was chosen based on the main reflection of the austenite (1 1 1) and martensite (1 1 0) phases.

The scale used in Figures 4 and 5 does not allow the clear perception of the austenitic and martensitic phases detection. It was comparing the superimposed diffraction patterns measured at different incidence angles, as Figure 6 presents, that it was established how to judge on which signal the phase was or was not first identified.

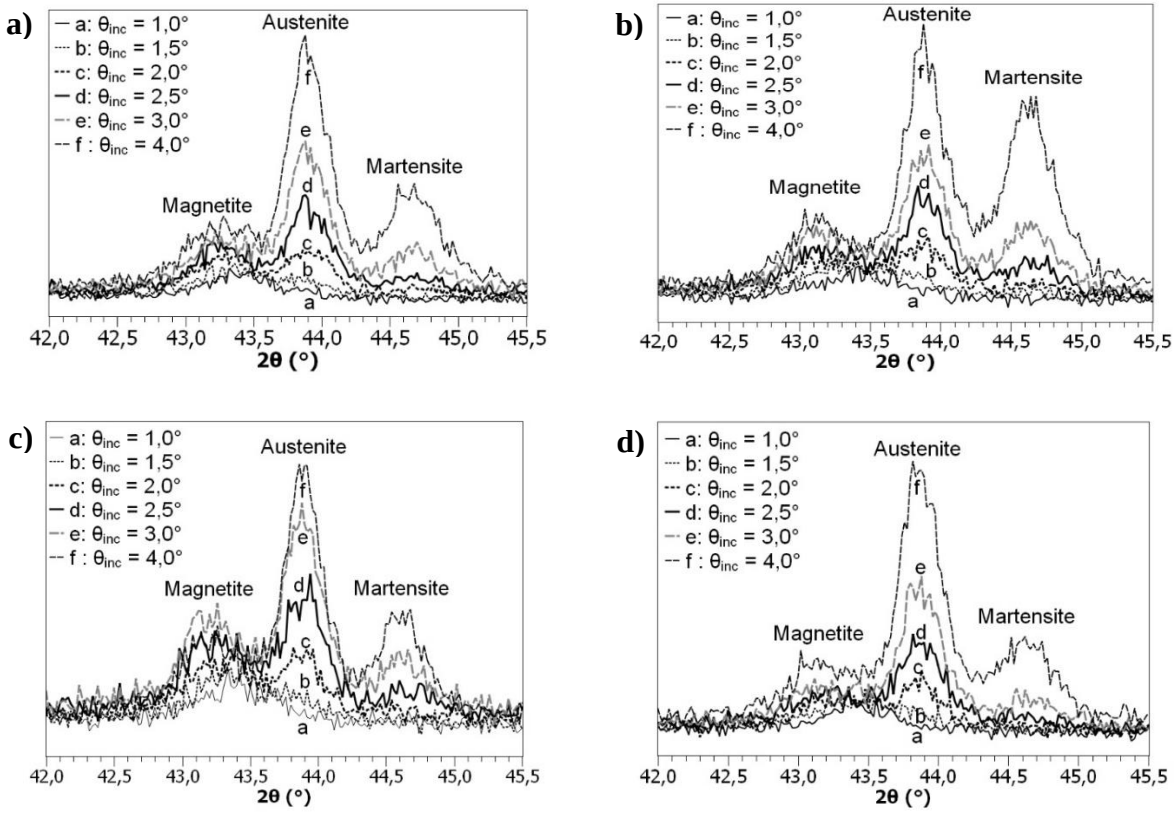

Figure 6: *Detail of the appearance of main reflections of austenite and martensite phases of a) TP, b) TS, c) BP and d) BS specimens.*

Based on Figure 6, Table 1 was organized and guided the comparative inferences about the thicknesses of the layers formed after the heat treatment. It seems also from Figure 6 that the peak position suffers a little shift. The explanation for these peak shifts for lower angles while incidence angles raise is related to the geometry asymmetry of the GIXRD and it is induced by refraction, as demonstrated by Toney & Brennan [15].

Table 1: Lowest incident angle at which austenite and martensite phases were first detected.

	Incident Angle			
Phase detected	**TP**	**TS**	**BP**	**BS**
Austenite	1.5°	1.5°	1.5°	2.0°
Martensite	2.5°	2.0°	2.5°	2.5°

Analyzing Table 1, some points were drawn:

1) Since for BS specimen the austenite phase was identified at $\theta_{inc} > 2.0°$, while for others it occurs at $\theta_{inc} > 1.5°$, the BS specimen must have the biggest oxide top layer.
2) The layer of austenite phase on TP and BP specimens must be bigger than on the sanded TS and BS specimens, since the difference between incidence angles at which the martensite and austenite appearance is bigger on the polished specimens (1.0°) than on the sanded ones (0.5°).
3) The BS specimen has the smaller austenite layer because besides presenting the smallest difference between the incidence angles on the martensite and austenite phases (0.5°), this difference is verified on larger angles when compared with TS, which implies a smaller depth difference for the same penetration of X-rays.
4) The TS specimen is the one that has the smallest total bilayer (oxide + austenite), since the martensite phase appears at the lowest incident angle (2.0°) measured, when compared with others that appear only at $\theta_{inc} > 2.5°$.

These conclusions are based on the hypothesis that the layers formed over the bulk for all samples have the same structure, same porosity, and constitution, without any significant difference in the orientation, distribution and size of crystallites. A simplified bilayer model was used to raise the conclusions above, since the absorption coefficient of hematite and magnetite phases are quite similar,

even having indications that suggest some differences, especially in the composition of the oxide layer, between the specimens.

Furthermore, one of the purposes of this work was to verify if the analysis by GIXRD would bring relevant information regarding the thicknesses of the layers without a destructive test, that requires a more careful sample preparation, like SEM analysis.

3.2. SEM results

In this section we will present only the electron micrographs performed with the maximum magnification used (15,000 ×), with both types of detectors (BSE and SE) to show how the effect of Z-contrast improves the differentiation of the layers. As discussed previously, however, only two micrographs performed with backscattered electrons detector were used to calculate the average thickness value of each layer.

Figures 7 and 8 evidenced SEM images of specimens treated on the top and bottom basket of the furnace, respectively. In the top of each figure is the bakelite mounting, followed by the cross section of the layers and the matrix. On the right side the micrographs were made by using SE detector, and, on the left, BSE detector.

The SEM micrographs showed that the layer formed during the oxidation process has a gap between the oxide and the austenite layers. This gap indicates the low adherence of the oxide layer formed during thermal aging, perhaps because during mounting process it got detached from the bulk. In order to evaluate the thickness of the bilayers this gap was disregarded, and an average value was obtained from 12 measurements made by BSE micrographs.

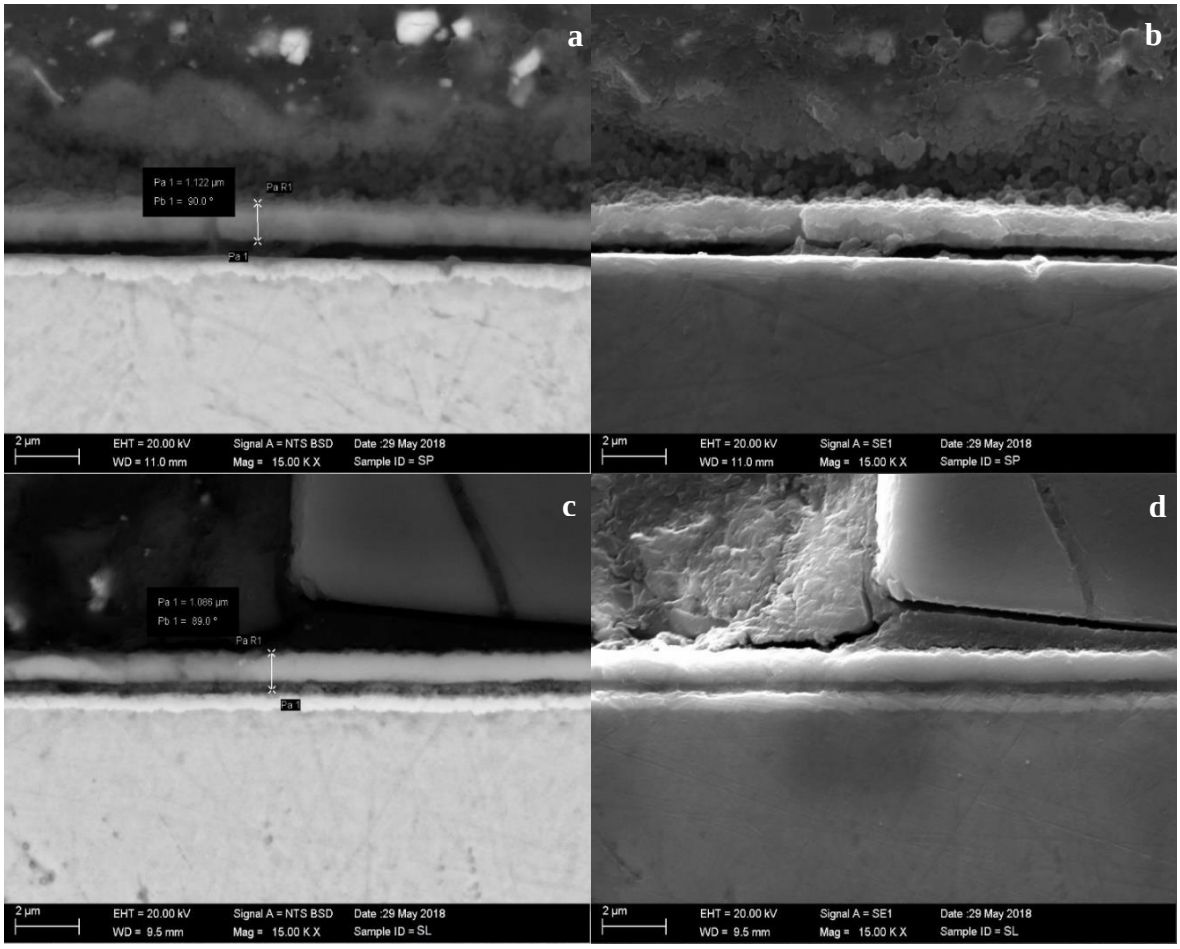

Figure 7: *SEM of TP (a & b) and TS (c & d) with 15,000× of magnification, using BSE detector (a & c) and SE detector (b & d).*

In BSE images (Figures 7 and 8), the bigger the atomic number of the layer's elements, the more backscattered electrons are generated from the sample and the clearer the respective micrograph's portion appears. This is known as z-contrast. So, the darker layer is associated with the mixture of oxides and the lighter one to the austenitic phase, which is stabilized by the migration of the iron from the matrix alloy to the oxide layer, generating this transition layer in which the heavier alloying elements (such as Nickel, Cobalt and Molybdenum) [4-5] exist in greater quantity than in the original bulk composition.

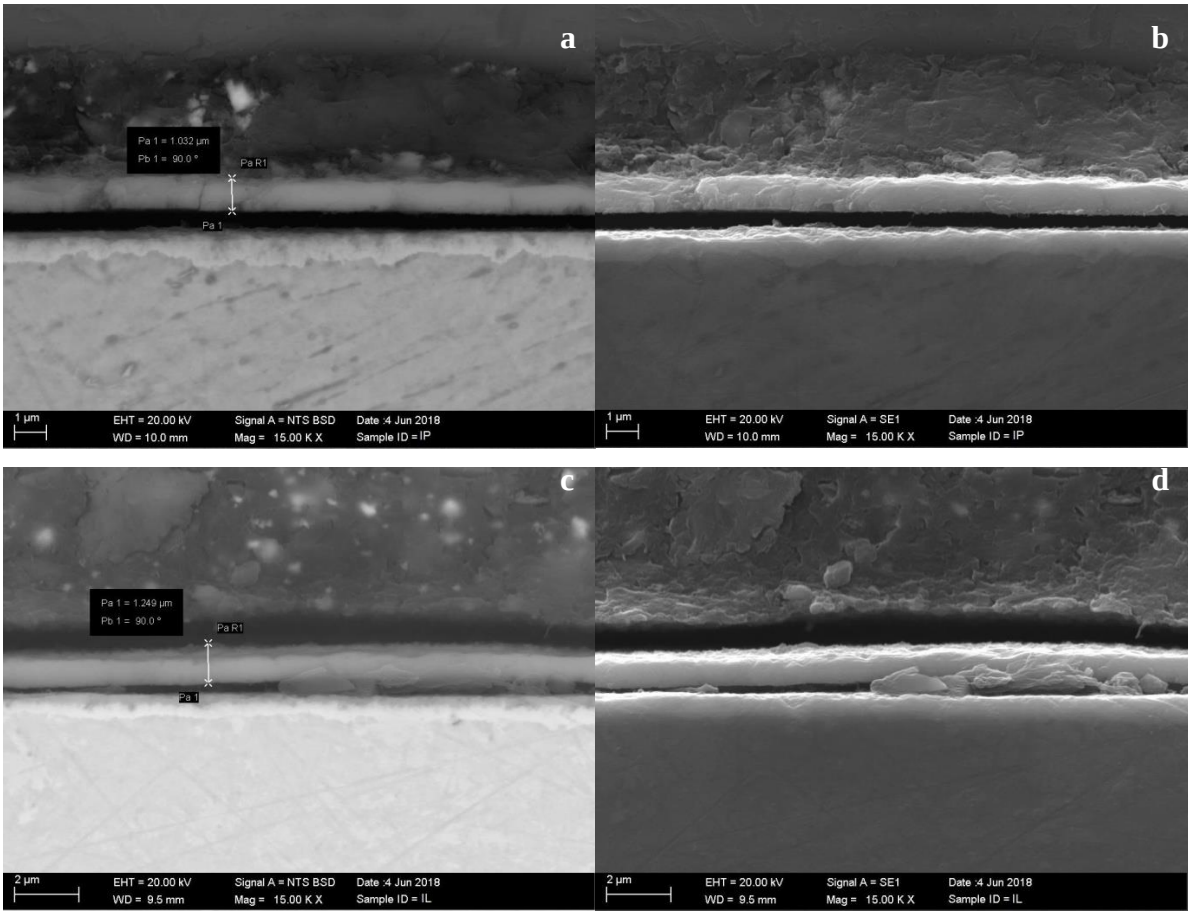

Figure 8: *SEM of BP (a & b) and BS (c & d) with 15,000× of magnification, by using BSE detector (a & c) and SE detector (b & d).*

Table 2 compiles the thickness values obtained by scanning electron microscopy, by using the methodology described in section 2.3. The average value of the top oxide layer found was (1.130 ± 0.094) µm and (0.507 ± 0.090) µm for austenite layer, which means that during this thermal aging approximately 69 % of the layer formed is constituted by the mixture of hematite and magnetite, and 31 % of austenite.

Table 2: Average thickness calculated from BSE micrographs.

SPECIMENS	OXIDE (µm)	AUSTENITE (µm)	BILAYER (µm)
TP	1.198 ± 0.044	0.509 ± 0.048	1.707 ± 0.065
TS	0.877 ± 0.039	0.427 ± 0.038	1.303 ± 0.054
BP	1.144 ± 0.040	0.749 ± 0.050	1.893 ± 0.064
BS	1.300 ± 0.061	0.344 ± 0.044	1.644 ± 0.075

The different surface finishes do not reveal any consistent conclusion, because although the polished samples exhibit bigger austenite layer thickness in comparison with the sanded ones, for specimens treated on the top basket of the furnace the oxide layer was bigger, and for the bottom position it was smaller.

If the conclusions raised by GIXRD results were compared with the thickness measurements compiled in Table 2, it can be seen that BS specimen has the biggest oxide layer (1.300 ± 0.061) μm, which is in agreement to the first conclusion by GIRXD, as well as the second one, since the polished specimens TP and BP have the largest austenite layer, and the BS the smallest one, in accordance with the third conclusion listed on section 3.1. Besides, the TS specimens have the smallest total layer of (1.303 ± 0.054) μm also in agreement with the previous results.

Therefore, crossing the results presented on Table 2 with the conclusions of GIXRD analysis confirms that qualitative and comparative conclusions can be drawn for specimens treated under the same conditions by GIXRD technique, and can be used to qualitatively evaluate the main thickness of a multi-layer structure, at least for oxide/metal bi-layers with thickness differences on the order of hundreds of nanometers and total size about a few micrometers.

4. CONCLUSION

The GIXRD technique was used to evaluate a layer formed onto samples of MA300 during an aging process in steam atmosphere for 6 h at 480 °C. Not only an outermost oxide layer composed of hematite and magnetite was formed onto the specimens but also an intermediate metallic layer with fcc cell structure could be identified throughout the use of this technique.

No significant conclusions could be drawn from the distinct surface finishes, because although the sanded specimens had presented lower austenite layers, on the other hand, no tendency was observed for the thickness of oxide layers.

The aspect that was most relevant in this work was that the analysis of the incidence angles at which each new phase was detected while θ_{inc} increases, allowed comparatively the qualitative evaluation of the layers thicknesses, and the conclusions extracted by using this methodology proved to be consistent, since SEM measurements of the layers thicknesses confirmed all of them.

It is still necessary to study more carefully the definition of the threshold of the incidence angle at which the appearance of a new phase is identified. However, by the results presented early, for this order of magnitude of thicknesses (about 1 to 2 μm) and in this case of oxide/metal bi-layer structure, it appears that the GIXRD technique can be used not only to identify and to order the layers formed, but also to evaluate the thickness of the layers in a comparative way.

ACKNOWLEDGMENT

The authors hereby acknowledge the support received from their Institution for the development of this work, especially that obtained from Ana Elis Lopes Claudio, who guided us to achieve our objective, and Odair Doná Rigo for the discussion, knowledge transference, and incentive during the accomplishment of this job.

REFERENCES

[1] MOURITZ, A. P. **Introduction to Aerospace Materials**, 1st ed. Cambridge: Woodhead Publishing, 2012.

[2] SHA, W.; GUO, Z. **Maraging Steels: Modelling of Microstructure, Properties and Applications**, 1st ed. New York: Woodhead Publishing, 2009.

[3] TEWARI, R.; MAZUMDER, S.; BATRA, I.; DEY, G.; BANERJEE, S. Precipitation in 18 wt% Ni maraging steel of grade 350. **Acta Materialia**, v. 48, p. 1187-1200, 2000.

[4] REZEK, J.; KLEIN, I. E.; YAHALOM, J. Structure and corrosion resistance of oxides grown on maraging steel in steam at elevated temperatures. **Applied Surface Science**, v. 108, p. 159-165,1997.

[5] KLEIN, I. E.; YANIV, A. E.; SHARON, J. The Oxidation Mechanism of Fe-Ni-Co Alloys. **Oxidation of Metals**, v. 16, p. 99-106, 1981.

[6] QUADAKKERS W. J.; ENNIS P. J.; ZUREK J. ; MICHALIK M. Steam oxidation of ferritic steels - laboratory test kinetic data. **Materials at High Temperatures**, v. 22, p. 47-60, 2005.

[7] ENNIS P. J.; QUADAKKERS W. J. Mechanisms of steam oxidation in high strength martensitic steels. **International Journal of Pressure Vessels and Piping**, v. 84, p. 75-81, 2007.

[8] LHOTKA, J.; KUZEL, R.; CAPPUCIO, G.; VALVODA, V. Thickness determination of thin polycrystalline film by grazing incidence X-ray diffraction. **Surface and Coatings Technology**, v. 148, p. 96-101, 2001.

[9] BROADHURST, A.; ROGERS, K. D.; LOWE, T. W.; LANE, D. W. Determination of depth-dependent diffraction data: a new approach. **Foundations of Crystallography**, v. A61, p. 139-146, 2005.

[10] SIMONEONE, D.; BALDINOZZI, G.; GOSSET, D.; ZALCZER, G.; BÉRAR, J. Rietveld refinements performed on mesoporous ceria layers at grazing incidence. **Journal of Applied Crystallography**, v. 44, p. 1205-1210, 2011.

[11] CULLITY, B. D.; STOCK, S. R. **Elements of X-Ray Diffraction**, 3rd ed. Harlow: Pearson Education Limited, 2014.

[12] KLAUS, M.; GENZEL, C. X-ray residual stress analysis on multilayer systems: an approach for depth-resolved data evaluation. **Journal of Applied Crystallography**, v. 46, p. 1266-1276, 2013.

[13] BIRKHOLZ, M. **Thin Film Analysis by X-Ray Scattering**, 1st ed. Weinheim: Wiley-VCH Verlag GmbH & Co. KGaA, 2006.

[14] MAGNEE, A.; DRAPIER, J. M.; COUTSOURADIS, D.; HABRAKAN, L.; DUMONT, J. **Cobalt-containing high-strength steels**. Brussels: Centre D'information Du Cobalt, 1974.

[15] TONEY, M. F.; BRENNAN, S. Observation of the effect of refraction on x rays diffracted in a grazing-incidence asymmetric Bragg geometry. **Physical Review B**, v. 39, p. 7963-7966, 1989.